

# Cross-correlation of the CMB and radio galaxies in real, harmonic and wavelet spaces: detection of the integrated Sachs-Wolfe effect and dark energy constraints

P. Vielva<sup>1</sup> E. Martínez-González<sup>2</sup> and M. Tucci<sup>2,3</sup>

<sup>1</sup>*Physique Corpusculaire et Cosmologie, Collège de France, 11 pl. M. Berthelot, F-75231, Paris Cedex 5, France*

<sup>2</sup>*Instituto de Física de Cantabria (CSIC - UC), Avda. Los Castros s/n, 39005, Santander, Spain*

<sup>3</sup>*Astrophysics Group, The Blackett Laboratory, Imperial College, London SW7 2AZ UK*

*e-mails : vielva@cdf.in2p3.fr, martinez@ifca.unican.es, m.tucci@imperial.ac.uk*

28 October 2018

## ABSTRACT

We report the first detection of the Integrated Sachs-Wolfe effect (ISW) in wavelet space, at scales in the sky around  $\theta \approx 7^\circ$  with a significance  $\approx 3.3\sigma$ , by cross-correlating the Wilkinson Microwave Anisotropy Probe (WMAP) first-year data and the NRAO VLA Sky Survey (NVSS). In addition, we present a detailed comparison among the capabilities of three different techniques for two different objectives: to detect the ISW and to put constraints in the nature of the dark energy. The three studied techniques are: the cross-angular power spectrum (CAPS, *harmonic space*), the correlation function (CCF, *real space*) and the covariance of the Spherical Mexican Hat Wavelet (SMHW) coefficients (CSMHW, *wavelet space*). We prove that the CSMHW is expected to provide a higher detection (in terms of the signal-to-noise ratio) of the ISW effect for a certain scale. On the other hand, the detection achieved by the CAPS is the lowest one, being the signal-to-noise ratio dispersed among a wide multipole range. The CCF provides an intermediate detection level. This prediction has been corroborated by the analysis of the data. The SMHW analysis shows that the cross-correlation signal is caused neither by systematic effects nor foreground contamination. However, by taking into account the information encoded in all the multipoles/scales/angles, the CAPS provides slightly better constraints than the SMHW in the cosmological parameters that define the nature of the dark energy. The limits provided by the CCF are wider than for the other two methods, although the three of them give similar confidence levels. Two different cases have been studied: 1) a flat  $\Lambda$ CDM universe and 2) a flat universe with an equation of state parameter that, although does not change with time, could take values different from -1. In the first case, the CAPS provides (for a bias value of  $b = 1.6$ )  $\Omega_\Lambda = 0.73^{+0.11}_{-0.14}$  (at  $1\sigma$  CL). Moreover, the CAPS rejects the range  $\Omega_\Lambda < 0.1$  at  $\approx 3.5\sigma$ , which is the highest detection of the dark energy reported up to date. In the second case, the CAPS gives  $\Omega_{DE} = 0.70^{+0.12}_{-0.20}$  and  $w = -0.75^{+0.32}_{-0.41}$  (at  $1\sigma$  CL). This is the first estimation of the equation of state of the dark energy made through the cross-correlation of the CMB and the nearby galaxy density distribution. It also provides an independent estimation from the one made by the WMAP team using CMB and LSS.

**Key words:** cosmic microwave background, cosmology: observations

## 1 INTRODUCTION

During the last decade, the study of the anisotropies of the cosmic microwave background (CMB) is being (probably) the most important source for understanding the universe. Since the first all-sky detection reported by COBE-DMR in 1992 (Smoot et al. 1992), many ground and balloon based experiments have been measuring the CMB anisotropies,

drawing (together with other astrophysical data like those provided by supernova) a flat universe whose evolution is dominated by the dark energy. This general picture has been recently confirmed by the first-year results of the NASA WMAP satellite (Bennett et al. 2003a, Spergel et al 2003), providing a strong confirmation of the fiducial  $\Lambda$ CDM model.

At this point, one of the most interesting questions is the confirmation of this fiducial model by other independent analysis. In that sense, the Integrated Sachs-Wolfe effect (ISW, Sachs & Wolfe, 1967) –that is produced by the time variation of the gravitational potential, in the linear regime– plays a crucial role since it provides either a direct indication of the presence of dark energy in the case of a flat universe or else the existence of spatial curvature (Peebles & Ratra 2003). Since WMAP has established strong constraints in the flatness of the universe (Bennett et al. 2003a), the detection of the ISW will imply the detection of the dark energy.

Many different cosmological models can be included within the dark energy concept: the standard inflationary model dominated by a cosmological constant (with an equation of state parameter  $w = -1$ ;  $p \equiv w\rho$ ) and alternative models dominated by a dark energy whose energy density is spatially inhomogeneous with negative pressure and evolving with time, like topological defects, quintessence models and phantom models (see for instance Melchiorri 2004 and references therein). However, there is not yet a convincing explanation for the origin and nature of the dark energy within the practical physics framework. Obviously, any information extracted from cosmological data, that could help to characterise it, is very valuable (for phenomenological aspects of dark energy see for instance Corasaniti 2004).

Crittenden & Turok (1996) firstly suggested that the ISW could be detected by cross-correlating the CMB with the nearby galaxy density distribution. The first attempt to detect the cross-correlation of the CMB and the galaxy density distribution was done by Boughn & Crittenden (2002) using the COBE-DMR map and the NRAO VLA Sky Survey (NVSS, Condon et al. 1998) data. In that work, no cross-correlation was found, concluding that a future experiment with better sensitivity and resolution was required in order to detect it. The first-year WMAP data has provided a unique tool to perform such correlation. Several groups have reported ISW detection at different significant levels. Boughn & Crittenden (2004) have correlated the WMAP data with two different tracers of the nearby universe: the hard X-ray data provided by the HEAO-1 satellite (Boldt 1987) and the NVSS data. They find a statistical significance of 1.8 - 2.8  $\sigma$  at scales lower than  $3^\circ$ . Nolta et al. (2004) have done an independent analysis of the WMAP and NVSS cross-correlation obtaining  $\Omega_\Lambda > 0$  at 95%. Fosalba & Gaztañaga (2003) find a cross-correlation between WMAP and the APM Galaxy survey (Maddox et al. 1990) at 98.8% significance level at scales  $\approx 4^\circ - 10^\circ$ . Fosalba et al. (2003) cross-correlated WMAP with the Sloan Digital Sky Survey (SDSS, Abazajian et al. 2004) finding a positive ISW signal at the  $3\sigma$  level and determining  $\Omega_\Lambda = 0.69 - 0.86$  ( $2\sigma$  CL). These two data sets were also analysed by Scranton et al. (2003)\*. Afshordi et al. (2004) have cross-correlated the galaxies from the Near-IR Two Micron All Sky Survey (2MASS, Skrutskie et al. 1997) finding an ISW signal at  $2.5\sigma$  level.

All the previous works have performed the cross-

correlation of the WMAP data and the nearby universe tracers using the cross-angular power spectrum (CAPS, e.g. Afshordi et al. 2004) and the correlation function (CCF, e.g. Boughn & Crittenden, 2002, 2004, Nolta et al. 2004). In the present paper, we propose an alternative to the *harmonic* and *real spaces* to perform the correlation of the WMAP and NVSS data sets: the *wavelet space*. The motivation for using wavelets is clear since the ISW signal provided by the CMB-galaxies cross-correlation takes place at scales between  $2^\circ - 10^\circ$  (Afshordi 2004). As it is well known, wavelets are very suitable tools for detecting signals with a characteristic scale: by filtering the data at a given scale, those structures having that scale are amplified, allowing for a most optimal detection. Therefore, the wavelet analysis of the cross-correlation will concentrate almost all the signal of the ISW detection in a small scale range, allowing for a fast and direct measure of its signal-to-noise. This is not possible neither for the CAPS nor the CCF, where all the information spread out among all the multipoles/angles must be considered to estimate the total signal-to-noise. This effect is even more important for the CAPS than for the CCF.

Since we expect that the common structures in CMB and galaxy surveys have roundish rather than elongated shapes, we propose the Spherical Mexican Hat Wavelet (SMHW) to study the cross-correlation. A natural statistic of the cross-correlation in wavelet space is the covariance of the SMHW coefficients (CSMHW) at each scale. Wavelets have been extensively used in many astrophysical and cosmological analyses. In the CMB field, they have been used to study the non-Gaussianity of the CMB (Pando et al. 1998, Hobson et al. 1999, Aghanim & Forni, 1999, Tenorio et al. 1999, Barreiro et al. 2000, Mukherjee et al., 2000, Barreiro & Hobson 2001, Cayón et al. 2001, 2003, Matínez-González et al. 2002, Vielva et al. 2004, Starck et al. 2004, Cruz et al. 2005, McEwen et al. 2005), the component separation problem (Cayón et al. 2000, Vielva et al. 2001a, b, 2003) and denoising (Sanz et al. 1999a, b). This work is the first application to the cross-correlation of CMB and other data sets.

In addition to the pure ISW detection, the CAPS, the CCF and the CSMHW can be exploited, by comparing the ISW signal with the one provided by different cosmological models, to put constraints in the nature of the dark energy: not only in the quantity of the dark energy ( $\Omega_{DE}$ ), but also in the equation of state parameter ( $w$ ).

The paper is organized as follows. In Section 2 we describe the analysed data sets (WMAP and NVSS). In Section 3 the three cross-correlation estimators (CAPS, CCF and CSMHW) are presented. The expected signal-to-noise ratio for the ISW detection for the CAPS, the CCF and the CSMHW is calculated in Section 4. The results are given in Section 5 and, finally, in Section 6 are the conclusions.

## 2 THE WMAP AND NVSS DATA SETS

The two data sets that have been used in order to perform the CMB-nearby universe cross-correlation are the Wilkinson Microwave Anisotropy Probe (WMAP, Bennett et al. 2003a and references therein) first-year data and the NRAO VLA Sky Survey (NVSS, Condon et al. 1998).

\* See Afshordi et al. (2004) for a critical discussion of the analysis done in Fosalba & Gaztañaga (2003), Fosalba et al. (2003) and Scranton et al. (2003)

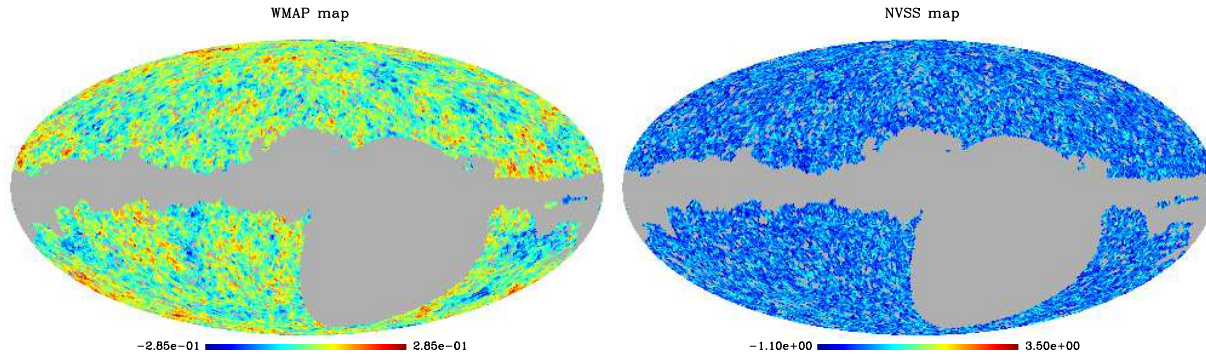


**Figure 1.** Analysed WMAP and NVSS data after the application of the *joint mask* and the subtraction of the residual monopole and dipole. The maps are represented in the HEALPix scheme, with a resolution parameter  $N_{side} = 64$  pixel size  $\approx 55$  arcmin).

## 2.1 WMAP data

The WMAP radiometers observe at five frequencies: 22.8, 33.0, 40.7, 60.8 and 93.5 GHz, having 1, 1, 2, 2 and 4 receivers per frequency band, respectively. All the papers, data and products generated by the WMAP team can be found in the Legacy Archive for Microwave Background Data Analysis (LAMBDA) Web site<sup>†</sup>. The WMAP maps are presented in the HEALPix scheme (Górski et al. 2005) at the  $N_{side} = 512$  resolution parameter. The WMAP team and other groups have proposed different CMB maps obtained from the WMAP data. In this work, we have used the map proposed by the WMAP team and already used by other groups (Komatsu et al. 2003, Vielva et al. 2004, Eriksen et al. 2004, Mukherjee & Wang 2003, Hansen et al. 2004, Cruz et al. 2005) for the study of the non-Gaussianity and the isotropy of the CMB. This map is generated (see Bennett et al. 2003b for details and Vielva et al. 2004 for a summarized description) as the noise weighted combination of all the maps produced by the receivers in which the CMB is the dominant signal (40.7, 60.8 and 93.5 GHz), after subtraction of the foreground emission and application of the so-called “Kp0” Galactic mask (defined by the WMAP team and where the brightest point sources are also masked). Whereas for the non-Gaussianity studies the resolution  $N_{side} = 256$  was commonly chosen, in the present work we have degraded the combined, corrected and masked map down to  $N_{side} = 64$  (pixel size  $\approx 55$  arcmin). The reason is that, as it was pointed out by Afshordi (2004), almost all the signal of the ISW is expected to be generated by structures with a scale larger than  $2^\circ$ . Hence, a WMAP resolution of around  $1^\circ$  is enough.

## 2.2 NVSS data

The NVSS catalogue covers around 80% of the sky and has flux and polarization measurements for almost 2 million of point sources with a minimum flux  $\approx 2.5$  mJy at 1.4 GHz. This catalogue has been already used for performing the correlation with the WMAP data (Boughn & Crittenden 2002,

2004 and Nolta et al. 2004). In this work, we have represented the point source catalogue in the HEALPix scheme, also at the  $N_{side} = 64$  resolution. Only the sources above 2.5 mJy have been used, which represents the 50% completeness (Condon et al. 1998). As it was pointed out by Boughn & Crittenden (2002) and Nolta et al. (2004), the mean density of point sources varies as a function of the declination. This systematic effect was corrected, by imposing that the mean of the galaxy density at each iso-latitude band is the same. The iso-latitude bands are defined taking into account the change in the RMS noise levels in the NVSS survey (see Figure 10 of Condon et al. 1998). Alternative strategies (as the one proposed by Nolta et al. 2004) were also considered, proving that results are not sensitive to the particular correction procedure.

As it was said before, the NVSS catalogue covers around 80% of the sky: for equatorial declination lower than  $-50^\circ$  there are not observations and, within the range  $-37^\circ > \delta > -50^\circ$  the coverage is not good enough. Hence, we only consider sources with an equatorial declination  $\delta \geq -37^\circ$ . With all these constraints, we have a galaxy distribution map of  $\approx 1600000$  radio sources with an average number of 40.4 counts per pixel.

In Figure 1 we have plotted the two maps to be analysed: WMAP (left) and NVSS (right). Both are in Galactic coordinates and the *joint mask* ( $Kp0 + \delta < -37^\circ$ ) has been applied. The residual monopole and dipole outside the mask have been removed.

## 2.3 Simulations

We have also performed realistic simulations in order to carry out the analysis. 1000 Gaussian simulations of the WMAP data have been done, following the concordance cosmological model given by the Table 1 of Spergel et al. 2003 ( $\Omega_\Lambda = 0.71$ ,  $\Omega_m = 0.29$ ,  $\Omega_b = 0.047$ ,  $H_0 = 72$ ,  $\tau = 0.166$ ,  $n = 0.99$ ) and using the CMBFAST code (Seljak & Zaldarriaga 1996). For each realization, we have simulated all the WMAP data measured by the receivers at 40.7, 60.8 and 93.5 GHz, they have been convolved with the real beams provided in the LAMBDA Web site, the anisotropic WMAP noise was added, the maps were combined using a noise-weighted average, the combined map was degraded to the  $N_{side} = 64$  resolution and the *joint mask* was applied. We

<sup>†</sup> Available at <http://cmbdata.gsfc.nasa.gov>

have cross-correlated the 1000 CMB simulations with the NVSS data, in order to evaluate the significance level of the cross-correlation obtained from WMAP and NVSS. This is enough to quantify the covariance matrix associated to random cross-correlations and we have checked that it is almost independent of the cosmological model used to simulate the CMB.

### 3 THE CROSS-CORRELATION ESTIMATORS: CAPS, CCF AND CSMHW

As it is well known (e.g. Peebles & Ratra 2003) for a flat universe where the dynamics are dominated by the dark energy, we expect a positive correlation between the CMB and the galaxy distribution of the nearby universe ( $z \lesssim 1$ , see for instance Afshordi 2004).

In this paper we apply three different techniques to study such correlation and to compare the performance of each of them for the detection of the ISW. The three studied techniques are the cross-angular power spectrum (CAPS), the correlation function (CCF) and the covariance of the SMHW coefficients (CSMHW), covering the *harmonic*, *real* and *wavelet spaces*. The CAPS has been already used, for instance, in Afshordi et al. (2004) to estimate the Sunyaev-Zeldovich, the point sources and the ISW signals by cross-correlating the 2MASS infrared source catalogue and WMAP. The CCF has been more extensively used, for instance in Boughn & Crittenden (2004) and Nolta et al. (2004). We proposed a new technique based in *wavelet space*, the CSMHW.

#### 3.1 The cross-angular power spectrum

The observed CAPS of WMAP and NVSS is given by:

$$\tilde{C}_{\ell WN} = \langle t_{\ell m} n_{\ell m}^* \rangle, \quad (1)$$

where  $t_{\ell m}$  and  $n_{\ell m}$  are the harmonic coefficients of the WMAP and the NVSS maps (respectively) and \* denotes complex conjugation.

This CAPS can be compared with the *theoretical* one expected from a given cosmological model:

$$\tilde{C}_{\ell}^{theo}{}_{WN} = p_{\ell}^2 b_{W\ell} b_{N\ell} M_{\ell, \ell'} C_{\ell'}^{theo}{}_{WN}, \quad (2)$$

where  $p_{\ell}$  is the pixel window function for the corresponding pixelization,  $b_{W\ell}$  and  $b_{N\ell}$  are the beam window function for WMAP and NVSS<sup>‡</sup>, respectively,  $M_{\ell, \ell'}$  is a coupling matrix that accounts for the *joint mask* (see Hivon et al. 2002) and  $C_{\ell}^{theo}{}_{WN}$  is the pure CAPS of WMAP and NVSS. Since  $N_{side} = 64$  resolution maps are analysed, only multipoles from  $\ell = 2$  to  $\ell = 191$  are considered. As it can be seen in, e.g., Nolta et al. (2004),  $C_{\ell}^{theo}{}_{WN}$  is given by:

$$C_{\ell}^{theo}{}_{WN} = 12\pi\Omega_m H_o^2 \int \frac{dk}{k^3} \Delta_{\delta}^2(k) F_{\ell}^W(k) F_{\ell}^N(k), \quad (3)$$

where  $\Omega_m$  is the matter density,  $H_o$  is the Hubble constant,  $\Delta_{\delta}^2(k) = k^3 P_{\delta}(k)/2\pi^2$  is the logarithmic matter power spectrum (being  $P_{\delta}(k)$  the matter power spectrum) and  $F_{\ell}^W(k)$

and  $F_{\ell}^N(k)$  are *filter functions* for the CMB and the galaxy density distribution, respectively, given by:

$$F_{\ell}^W(k) = \int dz \frac{dg}{dz} j_{\ell}(k\eta(z)) \quad (4)$$

$$F_{\ell}^N(k) = b \int dz \frac{dN}{dz} D(z) j_{\ell}(k\eta(z)) \quad (5)$$

In the case of  $F_{\ell}^W(k)$ , the integral is defined from  $z = 0$  to  $z$  at recombination epoch. The integration range for the *filter function*  $F_{\ell}^N(k)$  is defined, in practice, by the source redshift distribution function  $\frac{dN}{dz}$ . The function  $D(z)$  is the linear growth factor for the matter distribution (calculated from CMBFAST by computing the transfer function for different redshifts),  $g \equiv (1+z)D(z)$  is the linear growth suppression factor,  $j_{\ell}(k\eta(z))$  is the spherical Bessel function and  $\eta(z)$  is the conformal look-back time. The bias factor  $b$  is assumed to be redshift independent.

For the evolution of  $D(z)$  we consider the standard model dominated by a cosmological constant as well as alternative models dominated by a dark energy whose energy density is spatially inhomogeneous with negative pressure and evolving with time,  $\rho = \rho_0(1+z)^{3(1+w)}$ , where  $w$  is the equation of state parameter defined as the ratio of pressure to density. Whereas the standard inflationary model assumes  $w = -1$  and a homogeneous field (the cosmological constant), in general dark energy models are characterised by values of  $w < 0$ . For instance, topological defects can be phenomenologically represented by an equation of state parameter  $-1/3 \geq w \geq -2/3$  (see e.g. Friedland et al. 2003); quintessence models (Wetterich 1988, Caldwell et al. 1998) imply  $-1 < w < 0$  and phantom models have equation of state parameters  $w < -1$  (these last models, however, violate the null dominant energy condition; see Carroll et al. 2003 for a detailed discussion).

Although a convincing explanation for the origin and nature of the dark energy within the framework of particle physics is lacking, the models considered in the literature produce in general  $w$  varying with time. However, for most dark energy models, the equation of state changes slowly with time and a standard approximation assumes that (at least during a given epoch)  $w$  can be considered as an effective (and constant) equation of state parameter (Wang et al. 2000). Therefore, in this paper, we consider  $w$  constant as an useful approach to extract fundamental properties of the dark energy.

#### 3.2 The correlation function

The observed CCF is given by:

$$CCF(\theta) = \frac{1}{N} \sum_{\vec{n}, \vec{n}'} T(\vec{n}) N(\vec{n}'), \quad (6)$$

where  $T(\vec{n})$  and  $N(\vec{n})$  are the WMAP temperature and NVSS galaxy density (respectively) at position  $\vec{n}$ . The sum is extended over all the pixels that are allowed by the *joint mask* and inside a disk described by  $(\theta - \Delta\theta/2, \theta + \Delta\theta/2)$  where  $\vec{n}\vec{n}' = \cos(\theta)$  and  $\Delta\theta = 2^\circ$ . As in Nolta et al. (2004) the CCF is evaluated at 10 angles  $\theta = 1, 2, 3, 5, 7, 9, 10, 13, 15, 17$  and 19 degrees.

It can also be compared with the *theoretical* one ex-

<sup>‡</sup> For the NVSS galaxy density map there is no beaming, therefore  $b_{N\ell} = 1 \forall \ell$

pected from a given cosmological model:

$$\begin{aligned} CCF^{theo}(\theta) &= \left\langle \delta T(\vec{n}) \delta N(\vec{n}') \right\rangle \\ &= \sum_{\ell} \frac{2\ell+1}{4\pi} P_{\ell}(\vec{n}\vec{n}') p_{\ell}^2 b_{W\ell} b_{N\ell} C_{\ell}^{theo}_{WN}, \end{aligned} \quad (7)$$

where  $P_{\ell}(\vec{n}\vec{n}')$  are the *Legendre* polynomials and  $C_{\ell}^{theo}_{WN}$  is given by Equation 3.

### 3.3 The covariance of the wavelet coefficients

We define the CSMHW at a given scale  $R$  as:

$$Cov_{WN}(R) = \frac{1}{N_R} \sum_{\vec{p}} \omega_T(R, \vec{p}) \omega_N(R, \vec{p}), \quad (8)$$

where  $\omega_T(R, \vec{p})$  and  $\omega_N(R, \vec{p})$  are the SMHW coefficients of WMAP and NVSS (respectively) at position  $\vec{p}$ . We propose to study the cross-correlation of the WMAP and NVSS Spherical Mexican Hat Wavelet (SMHW) coefficient maps at different scales ( $R_1 = 50.0$ ,  $R_2 = 75.0$ ,  $R_3 = 100.0$ ,  $R_4 = 150.0$ ,  $R_5 = 200.0$ ,  $R_6 = 250.0$ ,  $R_7 = 300.0$ ,  $R_8 = 400.0$ ,  $R_9 = 500.0$ ,  $R_{10} = 600.0$ ,  $R_{11} = 750.0$ ,  $R_{12} = 900.0$ ,  $R_{13} = 1050.0$  arcmin) in the angular range where the ISW signal is expected to be more important (Afshordi 2004) for CMB-galaxy cross-correlations.

The SMHW coefficients are obtained by convolving the map with the SMHW at a given scale:

$$\omega_x(R, \vec{p}) = \int d\Omega' X(\vec{p} + \vec{p}') \Psi_S(\theta', R), \quad (9)$$

where  $\Psi_S(\theta', R)$  is the SMHW:

$$\Psi_S(y, R) = \frac{1}{\sqrt{2\pi}N(R)} \left[ 1 + \left(\frac{y}{2}\right)^2 \right]^2 \left[ 2 - \left(\frac{y}{R}\right)^2 \right] e^{-y^2/2R^2}, \quad (10)$$

being  $N(R)$  a normalization constant:

$$N(R) \equiv R \left( 1 + \frac{R^2}{2} + \frac{R^4}{4} \right)^{1/2}. \quad (11)$$

The distance on the tangent plane is given by  $y$  that is related to the latitude angle ( $\theta$ ) through:

$$y \equiv 2 \tan \frac{\theta}{2}. \quad (12)$$

The SMHW is obtained from the Euclidean Mexican Hat Wavelet (MHW) following the stereographic projection suggested by Antoine & Vanderheynt (1998). The reader is referred to the work of Martínez-González et al. (2002) where this projection is described for the SMHW, as well as its properties.

In Equation 8, the sum  $\sum_{\vec{p}}$  is extended over all the pixels that are not masked ( $N_R$ ). As it was already discussed in Vielva et al. (2004), since we are convolving a map with a large mask (the *joint mask* covers 43% of the sky) with the SMHW at a given scale  $R$ , we are introducing into the cross-correlation estimator  $Cov_{WN}(R)$  a large number of pixels – those close to the border of the mask – highly affected by the zero value of the mask, which implies a loss of efficiency. For that reason, at a given scale  $R$ , we *exclude* from the calculation of  $Cov_{WN}(R)$  all the pixels with a strong contamination from the *joint mask*. Whereas in Vielva et al. (2004) those pixels that were closer than  $2.5R$  to any one of the pixels of

the *joint mask* where excluded, for the present analysis we exclude only those pixels closer than  $1.0R$  to the *joint mask*. There are two reasons for that: first, the mask used in the present work is much larger than the one used in Vielva et al. (2004) and second, the number of pixels is lower, since the HEALPix resolution is 3 times lower. These two facts make the available number of data much smaller (for all the scales) than the ones in Vielva et al. (2004) and, therefore, we must be less restrictive in order to construct the 13 *exclusion masks*. However, we have checked that the ISW is also detected with the more restrictive *exclusion masks* proposed by Vielva et al. (2004).

The curve defined by Equation 8 can be easily compared with the theoretical CSMHW between the CMB and galaxy density distribution: the  $Cov_{WN}(R)$  is nothing more than the mean value of a map  $M(R) = \omega_T(R) \omega_N(R)$ , where the reference to the position  $\vec{p}$  has been removed for simplicity. It is straightforward to show that the theoretical wavelet cross-correlation can be written as:

$$Cov^{theo}_{WN}(R) = \sum_{\ell} \frac{2\ell+1}{4\pi} C_{\ell M}(R) \quad (13)$$

where  $C_{\ell M}(R)$  is the angular power spectrum of the map  $M(R)$  and it is given by:

$$C_{\ell M}(R) = p_{\ell}^2 s_{\ell}^2(R) b_{W\ell} b_{N\ell} C_{\ell}^{theo}_{WN}, \quad (14)$$

where, as before,  $p_{\ell}$  is the pixel window function for the corresponding pixelization,  $b_{W\ell}$  and  $b_{N\ell}$  are the beam window function for WMAP and NVSS,  $C_{\ell}^{theo}_{WN}$  is the pure CAPS of WMAP and NVSS and  $s_{\ell}(R)$  are the spherical harmonic coefficients of the SMHW at scale  $R$  (there is no dependence with  $m$ , since the SMHW is isotropic).

Summarising, the comparison of the experimental curves given by Equations 1, 6 and 8 with the theoretical prediction given by Equation 2, 7 and 13 can be done, by computing the *filter functions* and the pure CAPS for different cosmological models.

## 4 COMPARISON OF DIFFERENT TECHNIQUES: MOTIVATION FOR USING WAVELETS

The motivation for using wavelets for the detection of the ISW signal through the CMB-galaxies cross-correlation is given by the fact that such correlation has his maximum contribution in the scale range between  $2^{\circ}$  and  $10^{\circ}$  (see Afshordi 2004). As it is well known, wavelets are ideal tools for detecting signals (embedded in a given background) with a characteristic scale. The convolutions of the data with a wavelet with a certain scale, amplifies those structures with such scale, allowing for a most optimal detection.

In the present Section, we compare the expected signal-to-noise ratio of the cross-correlated signal between CMB fluctuations and the radio sources density distribution as a function of the angular scale for the estimators described in the previous section (see Figure 2): the cross-angular spectrum  $C_{\ell_{WN}}$  (CASP, Eq. 3); the correlation function (CCF, Eq. 7) and the covariance of wavelet coefficients  $Cov_{WN}(R)$  (CSMHW, Eq. 13). This is done for an ideal free-noise experiment with full-sky coverage and a resolution  $N_{side} = 64$  (and assuming no beaming, i.e.  $b_{W\ell} = b_{N\ell} = 1$ ).

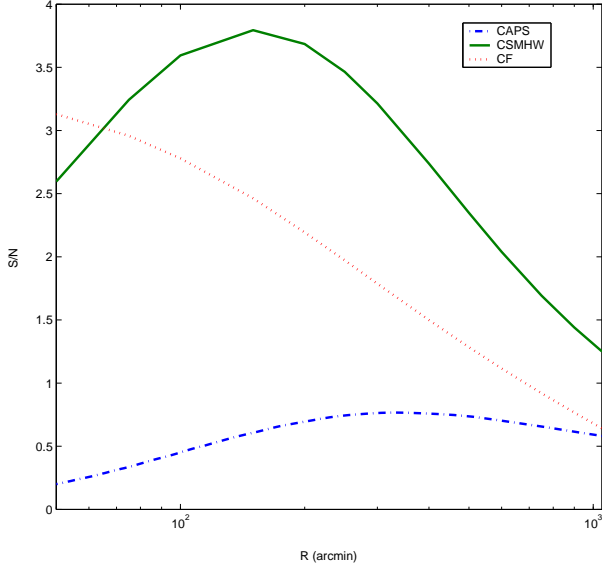


**Figure 2.** The expected signal-to-noise ratio of the CMB–radio sources cross-correlation according to the three studied techniques: the CSMHW (solid curve), the CAPS (dotted–dashed curve) and the CCF (dotted curve). The cosmological parameters are chosen according to the concordance model.

The signal-to-noise level can be estimated as the ratio between the cross-correlation estimator and its dispersion. As it is straightforward to show, the dispersion of the CAPS for two Gaussian random fields is given by:

$$\Delta C_{\ell}^{theo}_{WN} = \sqrt{\frac{C_{\ell}^{theo^2}_{WN} + C_{\ell}^{theo}_W C_{\ell}^{theo}_N}{2\ell + 1}} \quad (15)$$

where  $C_{\ell}^{theo}_W$  and  $C_{\ell}^{theo}_N$  are the angular power spectra for the CMB and the radio sources density distribution, respectively.

Using Equation 13 and 15, we find that the dispersion of the correlation of the CSMHW is given by:

$$\begin{aligned} \Delta Cov^{theo}_{WN}(R) &= \\ \sqrt{\langle Cov^{theo}_{WN}(R)^2 \rangle - \langle Cov^{theo}_{WN}(R) \rangle^2} &= \\ \sqrt{\sum_{\ell} \frac{2\ell + 1}{16\pi^2} p_{\ell}^4 s_{\ell}^4(R) (C_{\ell}^{theo^2}_{WN} + C_{\ell}^{theo}_N C_{\ell}^{theo}_W)} & \quad (16) \end{aligned}$$

Equivalently, the dispersion of the CCF is given by:

$$\begin{aligned} \Delta CCF^{theo}(\theta) &= \\ \sqrt{\langle CCF^{theo}(\theta)^2 \rangle - \langle CCF^{theo}(\theta) \rangle^2} &= \\ \sqrt{\sum_{\ell} \frac{2\ell + 1}{16\pi^2} p_{\ell}^4 P_{\ell}^2(\vec{n}\vec{n}') (C_{\ell}^{theo^2}_{WN} + C_{\ell}^{theo}_N C_{\ell}^{theo}_W)} & \quad (17) \end{aligned}$$

Figure 2 shows that the CSMHW gives the highest signal-to-noise ratio ( $\approx 3.5$ ), at scales of  $\approx 4^{\circ}$ . As expected, the maximum significance for the CCF ( $\approx 3$ ) is reached at the smallest scale. The signal-to-noise ratio for the CAPS is significantly lower than for the other ones and always below 1, with a shape nearly flat ( $\approx 0.6$ ).

Let us recall two important points. First, the values of the signal-to-noise ratio curves for both, the CSMHW coefficients and the CCF have a very high scale-to-scale correlation, whereas there is no correlation in the case of the CAPS. In principle, by taking into account all the scales and the full correlations, one should expect to get comparable detection levels in the three cases. However, we remark that, for a certain scale, the detection of the ISW given by the CSMHW is proven to be the highest. In other words, the whole information of the ISW has been extremely concentrated and amplified in a very narrow range of angular scales. This is undoubtedly very useful in a practical situation, like the one addressed in this paper.

Second, in the case of a noisy experiment, the signal-to-noise ratio should be lower than the one obtained under our ideal conditions. This will be much more important for an estimator as the CCF, since it has its maximum amplification at the smallest scale. On the contrary, the CSMHW and the CAPS are almost unaltered in this case, since the maximum amplification is reached at intermediate angular scales, where the noise is almost negligible. The same argument is also applied if beaming is included.

## 5 RESULTS

The results obtained from the cross-correlation of WMAP and NVSS are presented in this Section. In Subsection 5.1 we show the ISW detection at  $\approx 3.3\sigma$  provided by the CSMHW. The curves obtained for the CCF and the CAPS are also presented. In Subsection 5.2 we compare the obtained cross-correlation with different theoretical curves provided by different  $\Lambda$ CDM cosmological models, in order to constrain the value of  $\Omega_{\Lambda}$ . The performance of the three techniques (CAPS, CCF and CSMHW) is compared, showing that all of them provide compatible limits at  $1\sigma$  CL, being the CAPS and the CSMHW better than the CCF in order to reject a zero dark energy value. Both of them discard values of  $\Omega_{\Lambda} < 0.1$  with a significance  $> 3\sigma$ . In particular, the CAPS detect the presence of dark energy at  $3.5\sigma$ , which is the highest detection reported up to date by using the ISW. Finally, in Subsection 5.3 we extend the analysis in order to constrain the value of dark energy density and the equation of state parameter, finding again compatible values at  $1\sigma$  for the three statistics.

### 5.1 The Detection of the ISW

We have computed the SMHW coefficients of WMAP and NVSS maps at different scales, from 50 arcmin to  $17.5^{\circ}$  (which implies an approximate size in the sky from  $1.5^{\circ}$  to  $35^{\circ}$ ) and we have studied their cross-correlation. Acceptance intervals for the correlated signal at certain significance levels  $\alpha$  (32%, 5% and 1%) have been established at each scale using simulations. These acceptance intervals contain a probability  $1 - \alpha$  and the remaining probability is the same above and below the interval (i.e.  $\alpha/2$ ). The acceptance intervals have been determined by studying the CSMHW  $Cov_{WN}(R)$  at each scale independently and calculating the corresponding percentiles.

In Figure 3 we present the ISW detection. Scales  $R_5$ ,



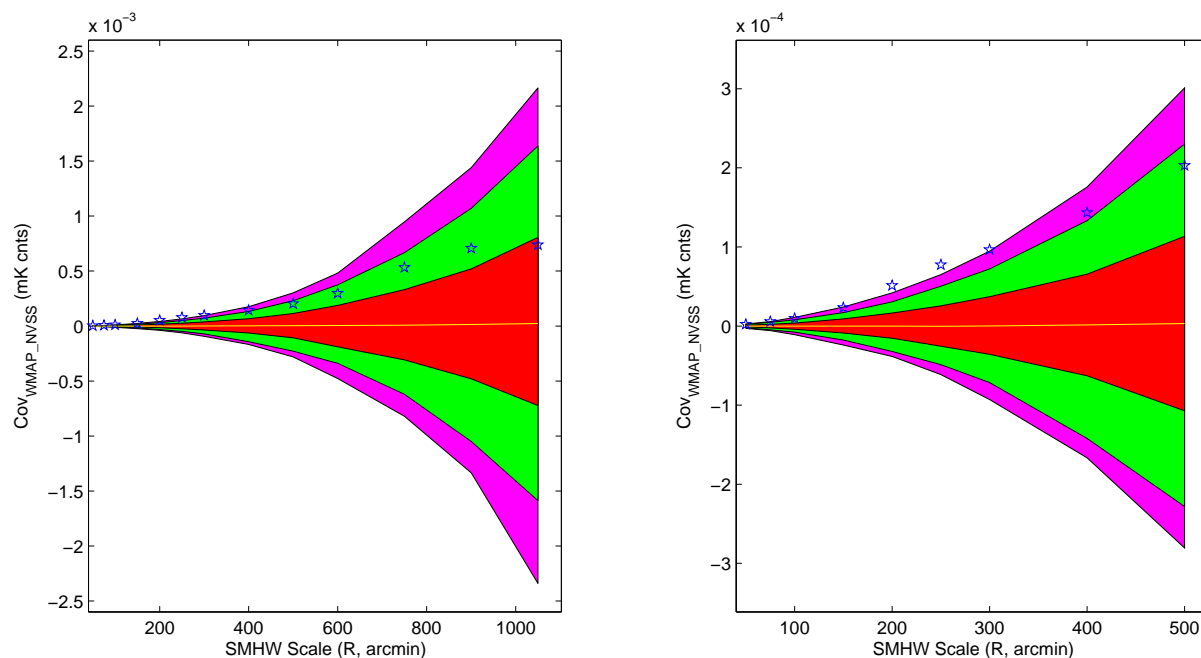


**Figure 3.** Cross-correlation in *wavelet space* of the WMAP and NVSS data (stars). Acceptance intervals for the 32% (inner interval), 5% (middle interval) and 1% (outer interval) significance levels are also plotted. The mean value of the cross-correlation for the 1000 simulations is also given (solid line). The plot is magnified for the lowest scales in the right panel.

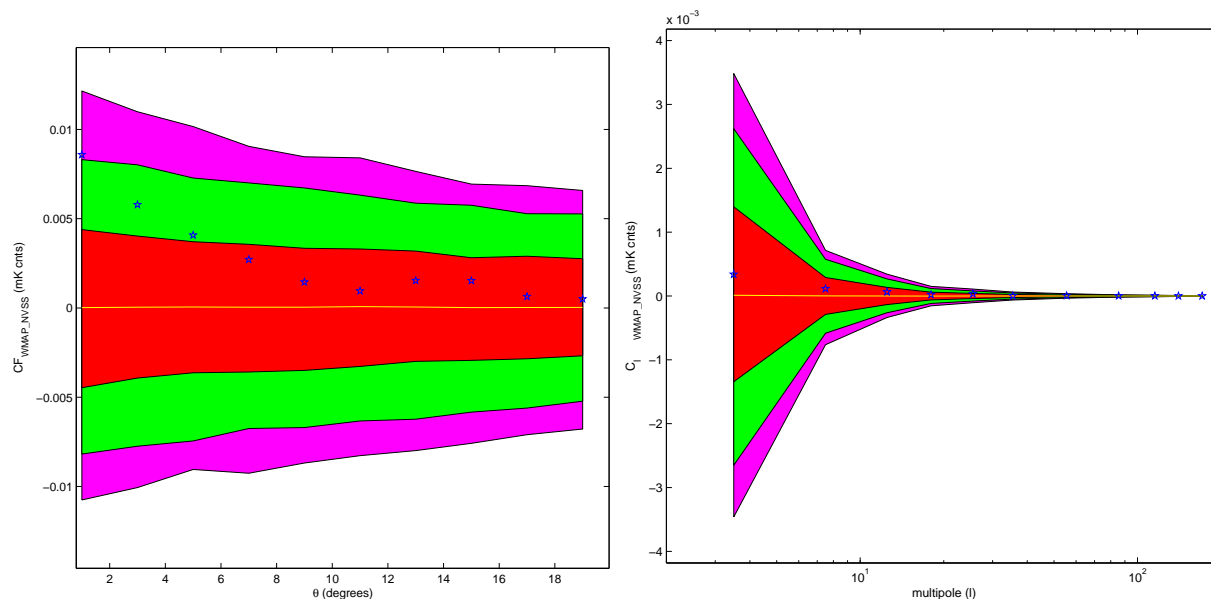


**Figure 4.** Cross-correlation in *real* (left panel) and *harmonic* (right panel) of the WMAP and NVSS data (stars). Acceptance intervals for the 32% (inner interval), 5% (middle interval) and 1% (outer interval) significance levels are also plotted. The mean value of the cross-correlation for the 1000 simulations is also given (solid line).

$R_6$  and  $R_7$  are outside the acceptance interval at 1% significance level (in particular, by increasing the number of simulations up to 10000, the scales  $R_5$  and  $R_6$  provide a detection at  $\approx 3.3\sigma$ ), representing a clear detection of the cross-correlation of the WMAP and NVSS data. These scales correspond to a size in the sky around  $6^\circ - 8^\circ$ , which is in very good agreement with the theoretical detection pre-

dicted in Section 4 and also with Afshordi (2004), that predicts an optimal scale for the ISW between  $2^\circ - 10^\circ$ .

For comparison, the detection curves for the CCF (left panel) and the CAPS (right panel) are given in Figure 4. The CCF provides a detection at  $\approx 95\%$ , in good agreement with the curves obtained by Boughn & Crittenden (2004) and Nolta et al. (2004). For a better visualization,

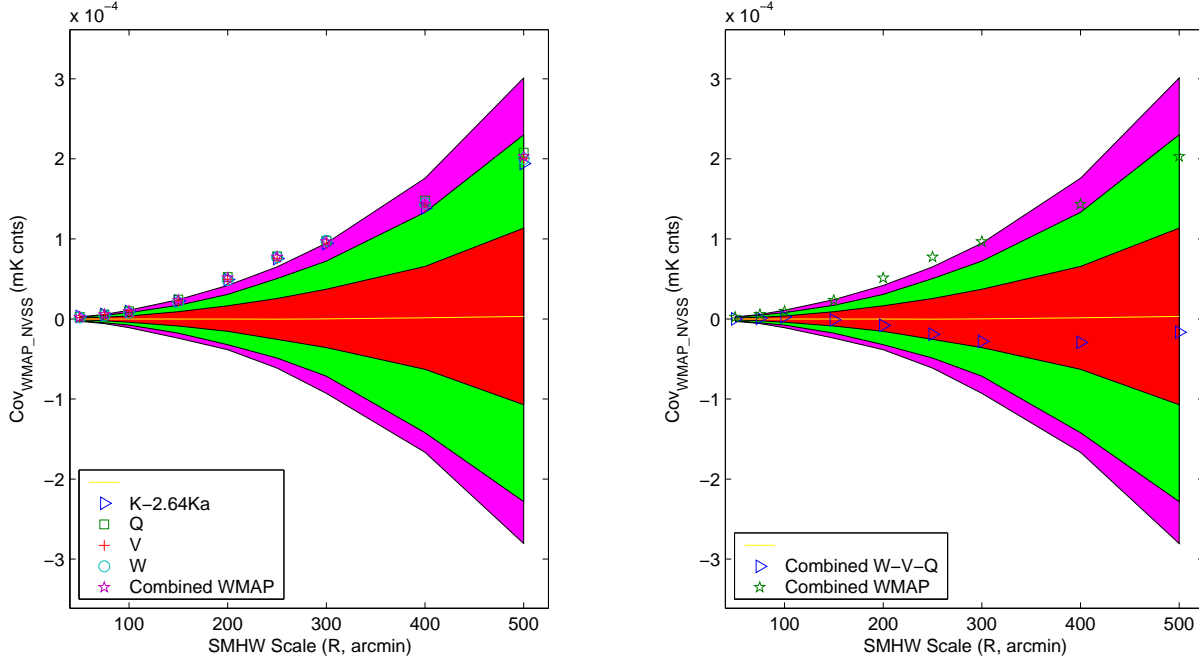


**Figure 5.** The left panel shows the CMB-nearby galaxy density correlation along the WMAP frequency range (W, V, Q, K - 2.64Ka and combined WMAP maps). The right panel shows the covariance between the noisy W-V-Q map and NVSS. The acceptance intervals are the same as the ones in Figure 3 since they are dominated by the cosmic variance.

the CAPS has been plotted after averaging multipoles in 11 intervals. As expected (see Figure 2), all the measured points are inside the acceptance interval at 32% significance level. We remark, as said in Section 4, that the CSMHW and the CCF curves are strongly correlated, whereas the correlation along the CAPS values is very small. This indicates that, by taking into account all the data and all the correlations in the proper way, the three techniques could provide a similar detection of the ISW, although differences are expected due to the presence of the mask. This will be considered in the next Subsections, when constraints in the nature of the dark energy are determined. Besides, due to the wavelet properties, almost the total signal of the ISW can be concentrated in a very specific scale range.

We have checked that this cross-correlation signal is not caused by systematic effects. We focus in the CSMHW detection, since is the one with the highest significance. In particular, the NVSS map has been also cross-correlated (independently) with each one of the WMAP receivers (Q1 and Q2 at 40.7 GHz, V1 and V2 at 60.8, W1, W2, W3 and W4 at 93.5 GHz). We found, for all the cases, the same CSMHW as for the combined WMAP map. We have also tested that the cross-correlations for the maps Q1-Q2, V1-V2 and W1-W2+W3-W4 with the NVSS data are compatible with simulations. For all these noisy maps, the CMB and foregrounds contributions are completely removed, showing no cross-correlation with the NVSS data. Hence, we conclude that all the WMAP receivers are producing the same cross-correlation signal and that it is not due to noisy artifacts.

We have also checked that the cross-correlation signal is not due to foreground emissions. In particular, the expected positive correlation between the radio sources pre-

sented both in the NVSS and the WMAP maps is considered. This correlation is expected to show a frequency dependence, reflecting the emission law of the point source population (e.g. Toffolatti et al. 1998). The cross-correlation curves for the different WMAP frequency channels (Q at 40.7 GHz, V at 60.8 GHz and W at 93.5 GHz) are shown in Figure 5. We have also considered the cross-correlation curve for the map K-2.64Ka, where K and Ka are the lowest frequency WMAP channels at 22.8 and 33.0 GHz, respectively. These channels are clearly contaminated by synchrotron emission. However, an additional CMB map can be generated by subtracting the Ka map from the K one, multiplying the first one by a factor of 2.64. This number corresponds to the expected increment of the synchrotron emission from 33 to 22.8 GHz<sup>§</sup>. As seen in the left panel of Figure 5, the same cross-correlation curve is obtained from the whole WMAP frequency range, showing not frequency dependence at all. Moreover, the cross-correlation curve for the W-V-Q map (free of CMB signal but with a clear foreground contribution) is perfectly compatible with zero (Figure 5, right panel). Hence, we conclude that the cross-correlation is only due to the CMB, with a negligible contribution from foregrounds, as expected for the ISW signal.

## 5.2 Constraints in $\Omega_\Lambda$

By comparing the measured detection with the theoretical curves for different cosmological models, limits on the

<sup>§</sup> A power law is assumed for the frequency dependence of the synchrotron emission:  $T_{syn}(\nu) \propto T_{syn}(\nu_0)(\nu/\nu_0)^{-2.7}$ , as proposed by Bennett et al. (2003b).



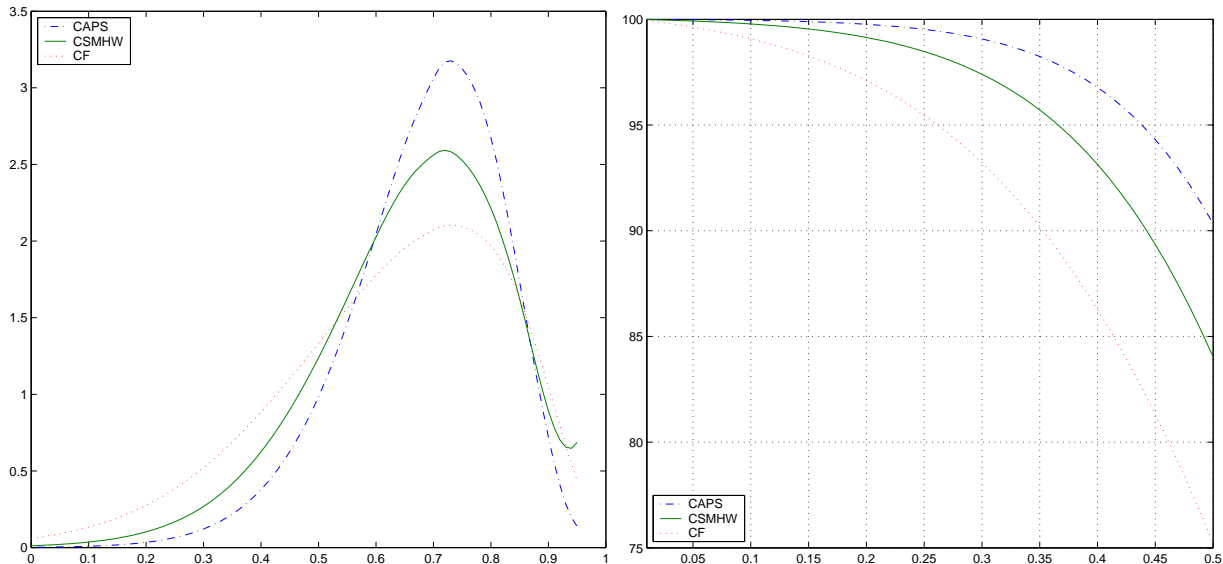


**Figure 6.** In the left panel, the likelihoods of the considered statistics (CAPS, CCF and CSMHW) are plotted as a function of  $\Omega_\Lambda$ . In the right panel we show the cumulative probability of having an  $\Omega_\Lambda$  greater than a certain value.

cosmological parameters can be established. In this first approach, we are interested in putting constraints on the amount of vacuum energy density  $\Omega_\Lambda$ , assuming a standard inflationary universe with  $w = -1$ , without redshift evolution. We have explored  $0 < \Omega_\Lambda < 0.95$ . For the bias parameter, we have considered the analysis of the NVSS catalogue (using the auto-correlation function) made by Boughn & Crittenden (2002, 2004) adopting the Dunlop & Peacock (1990) RLF1 model. They found that observations favor bias values of  $b = 1.3 - 1.6$ . For our analysis (where  $H_o = 0.72$  and  $\Omega_m = 0.29$ ),  $b = 1.6$  is the best value. In any case, we have checked that variations of the bias in the interval  $1.4 \leq b \leq 1.8$  do not change the results. The Dunlop & Peacock (1990) RLF1 model was also used to describe the  $dN/dz$  distribution since it fits well the NVSS galaxy auto-correlation, as it was already shown by Boughn & Crittenden (2002, 2004) and Nolta et al. (2004).

In practice, the observational curves for the CAPS, CCF and CSMHW (given by Equations 1, 6 and 8) are compared with the theoretical predictions (Equation 2, 7 and 13). For each statistic, a generalized  $\chi^2$  is defined:

$$\chi^2(p|b) = \Delta_{cross}^t(p|b; a_i) C(a_i, a_j)^{-1} \Delta_{cross}(p|b; a_j) \quad (18)$$

where the parameter  $p \equiv \Omega_\Lambda$  and  $\Delta_{cross}(a) = (cross_{WN}^{theo}(p|b; a) - cross_{WN}(a))$  is the difference between the observed CAPS/CCF/CSMHW and the theoretical prediction at scale  $a$  (i.e., the CSMHW  $R$  scale or the angular scale  $\theta$  of the CCF or the multipole  $\ell$  of the CAPS). The matrix  $C(a_i, a_j)$  is the correlation matrix of the WMAP and NVSS CAPS/CCF/CSMHW and it is obtained from 1000 simulations. Assuming that each  $C(a_i, a_j)$  is Gaussian distributed, a likelihood  $L \propto \exp(-\chi^2/2)$  can be calculated. The likelihood obtained for each statistic is represented in Figure 6 (left panel). At  $1\sigma CL$ , we obtain compatible constraints for the vacuum energy density:  $\Omega_\Lambda = 0.72_{-0.15}^{+0.12}$  (for

CSMHW),  $\Omega_\Lambda = 0.73_{-0.18}^{+0.12}$  (for CCF)<sup>¶</sup> and  $\Omega_\Lambda = 0.73_{-0.14}^{+0.11}$  (for CAPS).

On the right panel of Figure 6 we represent (for each statistic) the cumulative probability of having an  $\Omega_\Lambda$  greater than a certain value. This quantity provides us an alternative method to estimate the significance of the ISW detection. These plots show how the CAPS and the CSMHW are more powerful than the CCF for this purpose. There are several reasons for understanding this behaviour. On the one hand, the CAPS statistic has the important advantage that, apart from the mask effect, there are not correlations between multipoles, which is always a desirable property to build the chi-square, although all the available multipoles contribute in a similar way. On the other hand, although the CSMHW statistic has correlations among different scales, most of the signal is concentrated in a narrow angular range (that, in this case, is around several degrees), i.e. the most favourable condition to use wavelets. On the contrary, the CCF one has correlations among angular scales and, in addition, its maximum significance is smaller than the SMHW one. In particular, the CAPS provides  $\Omega_\Lambda > 0.1$  at a significance of  $\approx 3.5\sigma$ , which is the highest detection of the vacuum dark energy (based on the ISW) reported up to date.

The reason of those differences in the significance of the detection is due to the presence of a mask. In the case of full-sky data sets, a maximum likelihood method applied to the three quantities should give very similar results, since each

<sup>¶</sup> Notice that the likelihood obtained for the CCF is slightly different from the one given in Nolta et al. (2004, Figure 4d), although both provide consistent limits at  $1\sigma CL$ . There are differences that can explain it. First, in Nolta et al. (2004) the theoretical ISW effect is removed from the simulations to estimate the covariance matrix. Second, the estimate of the CCF is different in Nolta et al. (2004), since each pixel is weighted by taking into account the number of unmasked pixels at the original resolution.

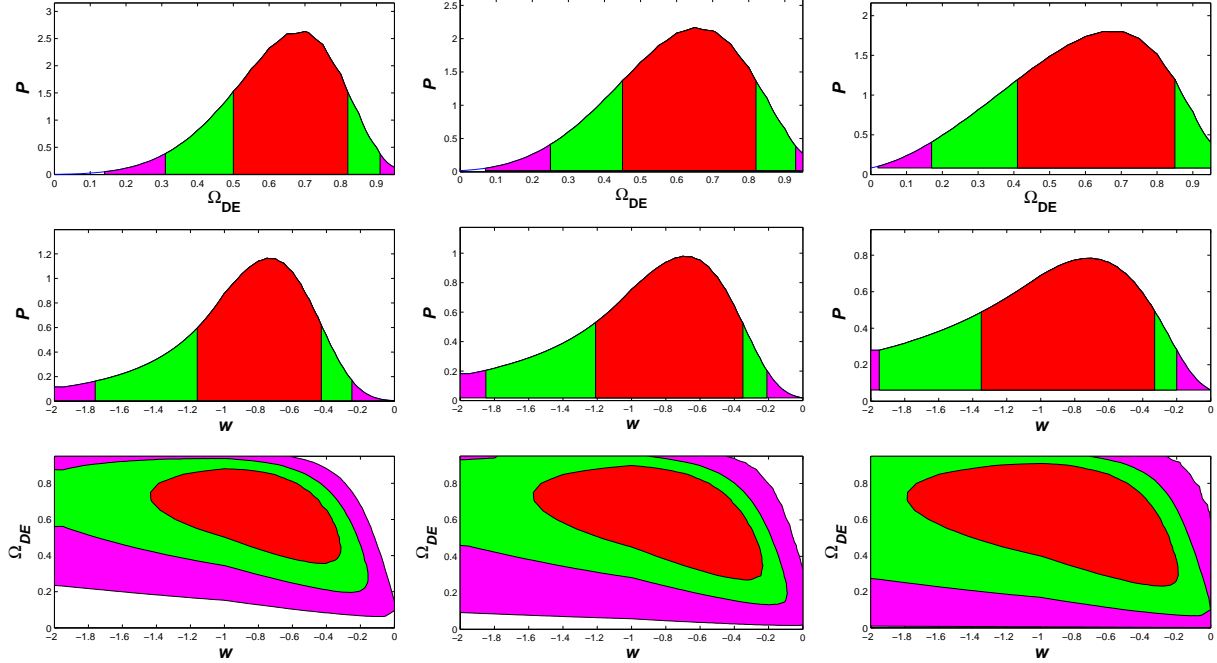


**Figure 7.** The logarithm of the marginalized pdf for  $\Omega_{DE}$  (upper) and  $w$  (middle) are presented. The 2D likelihood is also provided (bottom). The errors in the parameter estimation at  $1\sigma$ ,  $2\sigma$  and  $3\sigma$  are also plotted. First column shows the limits given by the CAPS, the second one is for the CSMHW and the last one is for the CCF.

of them can be expressed as a linear combination of any of the other two.

### 5.3 Constraints in $\Omega_{DE}$ and $w$

In the present section, we are interested in putting constraints in the nature of the dark energy. In particular, the amount of the dark energy density  $\Omega_{DE}$  (and so, the matter density, since we impose a flat universe) and the equation of state parameter  $w$  are studied. As it was done in the previous Section, we put limits in these cosmological parameters by comparing the measured WMAP and NVSS cross-correlation with the theoretical curves obtained from different cosmological models. The explored range for the dark energy density is  $0 < \Omega_{DE} < 0.95$ , whereas the one for the equation of state parameter is  $-2.0 < w < 0$ .

In this situation, a generalized  $\chi^2$  can be defined as in Equation 18, with parameters  $p \equiv (\Omega_{DE}, w)$ . As it was said in the Subsection 5.2, the elements of the correlation matrix are assumed to be Gaussian, hence we can define a likelihood as  $L \propto \exp(-\chi^2/2)$ . A joint pdf of the parameters  $f(\Omega_{DE}, w)$  can be calculated by normalizing the likelihood in the whole parameter space. The 2D likelihood is shown in Figure 7 (bottom panel). It is straightforward to calculate the marginalized pdf distributions  $f(\Omega_{DE})$  and  $f(w)$ . These marginalized pdfs are plotted in Figure 7 in the upper ( $f(\Omega_{DE})$ ) and in the middle ( $f(w)$ ) panels. The results for the CAPS, CSMHW and CCF are given in columns 1, 2 and 3, respectively.

We obtain at  $1\sigma$  CL:  $\Omega_{DE} = 0.70^{+0.12}_{-0.20}$  and  $w = -0.75^{+0.32}_{-0.41}$  with the CAPS;  $\Omega_{DE} = 0.70^{+0.15}_{-0.29}$  and  $w = -0.75^{+0.42}_{-0.60}$  with the CCF; and  $\Omega_{DE} = 0.65^{+0.17}_{-0.20}$  and  $w = -0.70^{+0.35}_{-0.50}$  with the CSMHW.

The limits in the dark energy density are compatible with the vacuum energy density calculated in the previous section. The constraints in  $w$  are less restrictive. The standard inflationary concordance model with  $\Omega_{DE} \approx 0.71$  and  $w = -1$  is perfectly compatible within the  $1\sigma$  CL. As explained in the previous Subsection, the differences in the results provided by the three statistics arise because of the presence of the mask.

## 6 CONCLUSIONS

We have performed the cross-correlation of the WMAP first-year data with the radio galaxy distribution traced by the NVSS catalogue, in the *harmonic*, *real* and *wavelet spaces*. This is the first application of wavelet techniques to study the cross-correlations between the CMB and the nearby universe. We found a clear cross-correlation at scales in the sky around  $\theta \approx 7^\circ$  with a significance  $\approx 3.3\sigma$ , in good agreement with theoretical predictions. Wavelets provide a better detection level respect to statistics based on spatial and harmonics space. This is due to the important advantage of wavelets to concentrate, in a particular and narrow scale range, almost the total signal of the ISW. On the other hand, the CAPS and the CCF provide a similar detection level only if the whole information spread along all the multi-poles/angles is properly combined and no mask is present.

Even more, by using the CSMHW, it is not required the calculation of different theoretical models, which are necessary to properly combine the whole information in the CAPS and CCF cases. The direct detection of the ISW obtained with the CSMHW is independent of the particular values for different parameters, as the bias, the point source red-

shift distribution, the equation of the state parameter of the dark energy, etc. The ISW detection at  $\approx 3.3\sigma$  is the highest significance level of the ISW reported up to date. By calculating the CSMHW for different combinations of the WMAP receivers, we have proven that this cross-correlation signal is not caused neither by systematic effects nor foreground contamination.

However, the comparison of the measured signal with the expected theoretical cross-correlation curves for different cosmological models, is needed to put constraints on the cosmological parameters. In particular, we have put limits to the amount of vacuum energy density  $\Omega_\Lambda$  (assuming  $w \equiv 1$ ), obtaining compatible constraints at  $1\sigma$  for the three different techniques: at  $1\sigma CL$ ,  $\Omega_\Lambda = 0.72^{+0.12}_{-0.15}$  (for CSMHW),  $\Omega_\Lambda = 0.73^{+0.12}_{-0.18}$  (for CCF) and  $\Omega_\Lambda = 0.73^{+0.11}_{-0.14}$  (for CAPS). Even more, the CAPS provides  $\Omega_\Lambda > 0.1$  at a significance of  $\approx 3.5\sigma$ , which is the highest detection of the vacuum dark energy (based on the ISW) reported up to date. We have used the bias parameter  $b = 1.6$  already calculated by Boughn & Crittenden (2002) for the NVSS data and the Dunlop & Peacock (1990) RLF1 model for the  $dN/dz$  distribution. Our results do not change for bias values in the interval  $1.4 \leq b \leq 1.8$ .

We have also tested the ability of the cross-correlation to put constraints on the nature on the dark energy by studying the amount of the dark energy  $\Omega_{DE}$  and the equation of state parameter  $w$ . We obtain  $\Omega_{DE} = 0.70^{+0.12}_{-0.20}$  and  $w = -0.75^{+0.32}_{-0.41}$  (at  $1\sigma$  CL) with the CAPS,  $\Omega_{DE} = 0.70^{+0.15}_{-0.29}$  and  $w = -0.75^{+0.42}_{-0.60}$  (at  $1\sigma$  CL) with the CCF and  $\Omega_{DE} = 0.65^{+0.17}_{-0.20}$  and  $w = -0.70^{+0.35}_{-0.50}$  (at  $1\sigma$  CL) with the CSMHW. Our estimation of the equation of state of the dark energy is the first one made through the cross-correlation of the CMB and the nearby galaxy density distribution. It provides an independent determination from that made by the WMAP team (Spergel et al. 2003) using CMB and LSS and by other groups (Caldwell & Doran 2004, Melchiorri 2004 and Corasaniti et al. 2004 and references therein) using, in addition to CMB and LSS, data coming from SN-Ia and/or BBN.

We remark that the differences found in the determination of the cosmological parameters are due to the presence of a mask. In the case of full-sky data sets, a maximum likelihood method applied to the three quantities should give very similar results, since each of them can be expressed as a linear combination of any of the other two.

Finally, in this paper we have shown that wavelets are a very promising tool for studying the correlation of the CMB with LSS data. Other effects like Sunyaev-Zeldovich or the contribution from point sources could also be studied having an appropriate LSS tracer.

## ACKNOWLEDGMENTS

We thank Martin Kunz for useful discussions on dark energy properties. We also acknowledge José L. Sanz and Belén Barreiro for very interesting comments. We are very thankful to Fernando Atrio-Barandela and Carlos Hernández-Monteagudo, for very useful comments regarding the NVSS data. We acknowledge the financial support provided through the European Community's Human Potential Program under contract HPRN-CT-2000-00124,

CMBNET, and partial financial support from the Spanish MEC projects ESP2002-04141-C03-01 and ESP2004-07067-C03-01. PV thanks IN2P3 (CNRS) for a post-doctoral contract. We acknowledge the use of LAMBDA, support for which is provided by the NASA Office of Space Science. This work has used the software package HEALPix (<http://healpix.jpl.nasa.gov>) developed by K. M. Górski, E. F. Hivon, B. D. Wandelt, J. Banday, F. K. Hansen and M. Barthelmann. We acknowledge the use of the software package CMBFAST (<http://www.cmbfast.org>) developed by U. Seljak and M. Zaldarriaga.

## REFERENCES

- Abazajian K. et al., 2004, AJ, 128, 502  
 Afshordi N., Loh Y.-S. & Strauss M. A., 2004, Phys. Rev. D, 69, 3524  
 Afshordi N., 2004, Phys. Rev. D, 70, 3536  
 Aghanim N. & Forni O., 1999, A&A, 347, 409  
 Antoine J. P. & Vanderheynt P., 1998, J. Math. Phys., 39, 3987  
 Barreiro R. B., Hobson M. P., Lasenby A. N., Banday A. J., Górski K. M. & Hinshaw G., 2000, MNRAS, 318, 475  
 Barreiro R. B. & Hobson M. P., 2001, MNRAS, 327, 813  
 Bennett C. L. et al., 2003a, ApJS, 148, 1  
 Bennett C. L. et al., 2003b, ApJS, 148, 97  
 Boughn S. P. & Crittenden R. G., 2002, Phys. Rev. Lett., 88, 21302  
 Boughn S. P. & Crittenden R. G., 2004, Nature, 427, 45  
 Boldt E., 1987, Phys. Rev., 146, 215  
 Caldwell R. R., Dave R. & Steinhardt P. J., 1998, Phys. Rev. Lett., 80, 1582  
 Caldwell R. R. & Doran P. J., 2004, Phys. Rev. D, 69, 3517  
 Carroll S. M., Hoffman M. & Trodden M., 2003, Phys. Rev. D, 68, 023509  
 Cayón L., Sanz J. L., Barreiro R. B., Martínez-González E., Vielva P., Toffolatti L., Silk J., Diego J. M. & Argüeso F., 2000, MNRAS, 315, 757  
 Cayón L., Sanz J. L., Martínez-González E., Banday A. J., Argüeso F., Gallegos J. E., Górski K. M., Hinshaw G., 2001, MNRAS, 326, 1243  
 Cayón L., Martínez-González E., Argüeso F., Banday A. J. & Górski K. M., 2003, MNRAS, 339, 1189  
 Condon J. J. et al., 1998, AJ, 115, 1693  
 Corasaniti P. S., 2004, PhD thesis, astro-ph/0401517  
 Corasaniti P. S., Kunz M., Parkinson D., Copeland E. J. & Bassett B. A., 2004, Phys. Rev. D, 70, 3006  
 Cruz M., Martínez-González E., Vielva P. & Cayón L., 2005, MNRAS, 356, 29  
 Crittenden R. G. & Turok N., 1996, Phys. Rev. Lett., 76, 575  
 Dunlop J. S. & Peacock J. A., 1990, MNRAS, 247, 19  
 Eriksen H. K., Hanse F. K., Banday A. J., Górski K. M. & Lilje P. B., 2004, ApJ, 605, 14  
 Fosalba P. & Gaztañaga E., 2004, MNRAS, 350, 37  
 Fosalba P., Gaztañaga E. & Castander F., 2004, ApJL, 597, 89  
 Friedland A., Murayama H. & Perelstein M., 2003, Phys. Rev. D, 67, 043519  
 Górski K. M., Hivon E., Banday A. J., Wandelt B. D., Hansen F. K., Reinecke M. & Bätterlmann M., 2005, ApJ, 622, 759  
 Hansen F., Banday A. J. & Górski K. M., 2004, MNRAS, 354, 641  
 Hivon E., Górski, K. M., Netterfield C. B., Crill B. P., Prunet S. & Hansen F., 2002, ApJ, 567, 2  
 Hobson M. P., Jones, A. W. & Lasenby A. N., 1999, MNRAS, 309, 125  
 Komatsu E. et al., 2004, ApJS, 148, 119

- McEwen J. D., Hobson M. P., Lasenby A. N. & Mortlock D. J., 2005, *MNRAS*, 359, 1583
- Maddox S. J., Efstathiou G. Sutherland W. J. & Loveday J., 1990, *MNRAS*, 242, 43
- Martínez-González E., Gallegos J. E., Argüeso F., Cayón L. & Sanz J. L., 2002, *MNRAS*, 336, 22
- Melchiorri A., 2004, astro-ph/0406652
- Mukherjee P., Hobson M. P. & Lasenby A. N., 2000, *MNRAS*, 318, 1157
- Mukherjee P. & Wang Y., 2004, *ApJ*, 613, 51
- Nolta M. R. et al., 2004, *ApJ*, 608, 10
- Pando J. et al., 1998, *Phys. Rev. Lett.*, 81, 4568
- Peebles P. J. E. & Ratra B., 2003, *Rev. Mod. Phys.*, 75, 599
- Scranton R. et al., 2003, astro-ph/0307335
- Seljak U. & Zaldarriaga M., 1996, *ApJ*, 469, 437.
- Smoot G. F. et al., 1992, *ApJL*, 396, L1
- Sachs R. K. & Wolfe A. M., 1967, *ApJ*, 147, 73
- Sanz J. L., Argüeso F., Cayón L., Martínez-González E., Barreiro R. B. & Toffolatti L., 1999a, *MNRAS*, 309, 672
- Sanz J. L., Barreiro R. B., Cayón L., Martínez-González E., Ruiz G. A., Díaz F. J., Argüeso F., Silk J. & Toffolatti L., 1999b, *A&AS*, 140, 99
- Spergel D. N. et al., 2003a, *ApJS*, 148, 175
- Starck J.-L., Aghanim N. & Forni O., 2004, *A&A*, 416, 9
- Tenorio L., Jaffe A. H., Hanany S. & Lineweaver C. H., 1999, *MNRAS*, 310, 823
- Toffolatti, L., Argueso Gomez, F., de Zotti, G., Mazzei, P., Franceschini, A., Danese, L. & Burigana, C., 1998, *MNRAS*, 297, 117
- Vielva P., Martínez-González E., Cayón L., Diego J. M., Sanz J. L. & Toffolatti L., 2001a, *MNRAS*, 326, 181
- Vielva P., Barreiro R. B., Hobson M. P., Martínez-González E., Lasenby A. N., Sanz J. L. & Toffolatti L., 2001b, *MNRAS*, 328, 1
- Vielva P., Martínez-González E., Gallegos J. E., Toffolatti L. & Sanz J. L., 2003, *MNRAS*, 344, 89
- Vielva P., Martínez-González E., Barreiro R. B., Sanz J. L. & Cayón L., 2004, *ApJ*, 609, 22
- Wang L., Caldwell R. R., Ostriker J. P. & Steinhardt P. J., 2000, *ApJ*, 530, 17
- Wetterich C., 1988, *Nucl. Phys. B*, 668, 1988

This paper has been produced using the Royal Astronomical Society/Blackwell Science  $\LaTeX$  style file.